PNAS

Supporting Information for

Neural functional theory for inhomogeneous fluids: Fundamentals and applications

Florian Sammüller, Sophie Hermann, Daniel de las Heras, and Matthias Schmidt

Florian Sammüller.
E-mail: florian.sammueller@uni-bayreuth.de
Matthias Schmidt.
E-mail: Matthias.Schmidt@uni-bayreuth.de

This PDF file includes:

Supporting Information Text

Higher-order correlations. Analogous to Sec. B.1, we demonstrate that higher-order correlations can be obtained from the neural correlation functional by nested automatic differentiation. This is due to the fact that the hierarchy of direct correlation functions $c_n(\mathbf{r},\mathbf{r}',\ldots,\mathbf{r}^{(n-1)};[\rho])$, $n\geq 2$, is accessible from successive functional derivatives of the one-body direct correlation functional (1),

$$c_n(\mathbf{r},\mathbf{r}',\ldots,\mathbf{r}^{(n-1)};[\rho]) = \frac{\delta^{n-1}c_1(\mathbf{r};[\rho])}{\delta\rho(\mathbf{r}')\ldots\delta\rho(\mathbf{r}^{(n-1)})}. \quad [1]$$

As illustrated in the main text, translational symmetry can be applied in bulk fluids such that the resulting bulk correlation function $c_n^b(\mathbf{r},\ldots,\mathbf{r}^{(n-2)}) = c_n(0,\mathbf{r},\ldots,\mathbf{r}^{(n-2)};[\rho_b])$ only incorporates $n-2$ remaining position coordinates.

We specialize again to the planar geometry of our neural functional and show in Fig. S1 the three-body bulk correlation function $\bar{c}_3^{b\star}(x,x')$ for a bulk density of $\rho_b = 0.7\sigma^{-3}$. While the computation of $\bar{c}_2^{b\star}(x)$ is practically immediate via a single reverse mode autodifferentiation pass, going to the three-body correlation function comes at the price of having to evaluate the Hessian of $c_1^\star(x;[\rho])$, for which different strategies exist (2). In principle, one can proceed by nesting autodifferentiation layers to obtain further members of the hierarchy Eq. (1), albeit being restricted by the practicability of the actual evaluation and the efficacy of the result. Note that the computational effort at the three-body level is by no means restrictive and that growing numerical demands are expected when considering higher-order correlations. The computation and analysis of $\bar{c}_3^b(x,x')$ might be especially useful for more complex fluid models, e.g. containing internal three-body interactions (3).

We compare $\bar{c}_3^{b\star}(x,x')$ to analytic approximations based on FMT. For both the Rosenfeld and the White Bear MkII functional, the three-body bulk direct correlation function is analytic in Fourier space. We point the reader to Ref. (4) for an expression of the original Rosenfeld result in terms of vectorial weight functions and to Refs. (5, 6) for an equivalent representation via scalar weights. As the weight functions remain unchanged, the White Bear MkII result follows immediately from the modification of the excess free energy density as laid out in Ref. (7).

A cumulant expansion of the bulk result of the three-body direct correlation function in Fourier space can be transformed to real space analytically, which in planar geometry gives

$$\bar{c}_3^b(x,x') = -\frac{bR^4}{a}\exp\left(\frac{-x^2+xx'-x'^2}{aR^2}\right), \quad [2]$$

where the width parameter a and the prefactor b are determined by

$$a = \frac{\nu}{\kappa}\frac{3}{5}\frac{53-25\eta+8\eta^2}{30+2\eta+5\eta^2-\eta^3}, \quad [3]$$

$$b = \kappa\frac{8\pi}{3\sqrt{3}}\frac{30+2\eta+5\eta^2-\eta^3}{(1-\eta)^5}, \quad [4]$$

with the packing fraction $\eta = \pi\rho_b/6$. The correction factors ν and κ are set to unity in the Rosenfeld FMT and attain the forms

$$\nu = \frac{53-35\eta+\eta^2+5\eta^3}{53-25\eta+8\eta^2}, \quad [5]$$

$$\kappa = \frac{30-6\eta}{30+2\eta+5\eta^2-\eta^3}, \quad [6]$$

in the White Bear MkII case.

The comparison reveals that the form of the neural three-body bulk correlation function $\bar{c}_3^{b\star}(x,x')$ is plausible and that it captures genuine features which go beyond both FMT descriptions. The Rosenfeld FMT yields a large discrepancy in the core region $x,x'\approx 0$, which is significantly unterestimated as compared to the results from the neural functional and from the White Bear theory. We recall that, as in Sec. C.2, the tensorial weights of Tarazona (8) have not been used in the FMT functionals and that their inclusion might be particularly relevant on the level of higher-order correlations. In this vein, investigating members of the direct correlation hierarchy Eq. (1) with the neural correlation functional could be a valuable aid for testing and refining analytic FMT functionals.

Spatial symmetry of the neural two-body direct correlation functional. A further consistency test of $c_2^\star(x,x';[\rho])$ arises due to its expected symmetry with respect to an interchange of the planar position coordinates x and x'. Recall that the excess free energy functional $F_{\mathrm{exc}}[\rho]$ generates the two-body direct correlation function according to

$$c_2(\mathbf{r},\mathbf{r}';[\rho]) = -\frac{\delta^2\beta F_{\mathrm{exc}}[\rho]}{\delta\rho(\mathbf{r})\delta\rho(\mathbf{r}')}, \quad [7]$$

see Eq. (2) and Eq. (4) of the main text. One can directly recognize from the symmetry of the second functional derivative in Eq. (7) that $c_2(\mathbf{r},\mathbf{r}';[\rho]) = c_2(\mathbf{r}',\mathbf{r};[\rho])$ must hold.

On the basis of the neural direct correlation functional in planar geometry, assessing the validity of the identity

$$c_2^\star(x,x';[\rho]) = c_2^\star(x',x;[\rho]) \quad [8]$$

is a highly nontrivial test. This is due to the fact that $c_2^\star(x,x';[\rho])$ evaluated at certain positions x and x' follows from automatic differentiation of $c_1^\star(x;[\rho])$, where the input density window is centered around the location x, see Sec. B.1. On the other hand, when formally evaluating $c_2^\star(x',x;[\rho])$, where the arguments x and x' are now reversed, the density window is centered around x', hence constituting a generally very different and a priori unrelated input profile. One can expect Eq. (8) to be recovered only if the physical implications of Eq. (7) are captured correctly by the neural functional. Note that Eq. (8) is a necessary condition for the existence of a unique neural excess free energy functional $F_{\mathrm{exc}}^\star[\rho]$, which can practically be obtained via functional line integration, see Sec. B.3. We exemplify in Fig. S2 that the neural two-body direct correlation functional $c_2^\star(x,x';[\rho])$ obtained via autodifferentiation of $c_1^\star(x;[\rho])$ indeed satisfies the symmetry requirement Eq. (8) to very high accuracy.

Neural equation of state for hard disks via dimensional crossover. Although the neural functional $c_1^\star(x;[\rho])$ was acquired explicitly for the three-dimensional hard sphere fluid, dimensional crossover techniques can be used to obtain bulk results for the two-dimensional hard disk system. This is facilitated by investigating the behavior of the hard sphere fluid under narrow confinement, which constitutes a quasi-two-dimensional scenario. With this method, one obtains the equation of state for the hard disk fluid from $c_1^\star(x;[\rho])$, as we demonstrate in the following.

We proceed similar to Sec. B.3 and utilize Eq. (16) to express the pressure $P(\rho_b)$ via the excess free energy density $\psi_b(\rho_b)$, which we aim to compute for a range of bulk densities ρ_b. Whereas $c_1^\star(x;[\rho])$ was evaluated for the three-dimensional bulk fluid at spatially constant density, cf. Eq. (15), here a suitable density profile $\rho_{2\mathrm{D}}(x)$ is constructed as input to the neural direct correlation functional in order to emulate narrow planar confinement. For this, we choose

$$\rho_{2\mathrm{D}}(x) = \frac{\rho_b}{x_w}\Theta\left(\left|x-\frac{x_w}{2}\right|\right) \qquad [9]$$

with the Heaviside function $\Theta(\cdot)$; note that Eq. (9) is a Dirac series and yields the Dirac distribution for $x_w \to 0$. The neural direct correlation functional is then evaluated at the center of this assumed slit, and the values $c_1^\star(0;[\rho_{2\mathrm{D}}])$ are used analogous to Sec. B.3 for the determination of $P_{2\mathrm{D}}^\star(\rho_b)$. The equation of state for the associated two-dimensional hard disk system follows formally for $x_w \to 0$. As this limit is not directly accessible in practice, we assess the obtained values for finite but small slit widths $0.3 \leq x_w/\sigma \leq 1$ and extrapolate to $x_w = 0$ via a quadratic fit.

The resulting equation of state $P_{2\mathrm{D}}^\star(\rho_b)$ for the two-dimensional hard disk fluid as obtained from this dimensional crossover on the basis of the neural network is shown in Fig. S3. We additionally display analytic equations of state from scaled particle theory (9) and by Henderson (10) which serve as reference. One recognizes that reasonable results can be achieved for low and medium densities, but that deviations to analytic results become noticeable for $\rho_b > 0.7\sigma^{-2}$. Nevertheless, it is both surprising and reassuring that the neural functional is capable of predicting correlations in narrow confinement, as no such situations were explicitly included in the training data. Recall that hard walls were imposed only at the borders of the simulation box of length $L = 20\sigma$ and that the inhomogeneous external potential within the simulation domain consisted solely of Fourier modes and of piecewise linear functions, cf. Eq. (3) in the main text. Presumably, improvements over the results presented in Fig. S3 could be obtained especially for large densities by including situations of very narrow confinement explicitly in the training data. From our outset, the successful achievement of a viable two-dimensional equation of state serves as a demonstration that $c_1^\star(x;[\rho])$ indeed captures the intricate functional relationship of the underlying physical problem instead of acting as a mere interpolation tool with respect to the encountered training data.

Neural DFT for the Lennard-Jones fluid. We illustrate the generalizability of our machine learning framework to other particle types by considering the truncated Lennard-Jones fluid with pairwise interparticle potential

$$\phi(r) = \begin{cases} 4\epsilon\left[\left(\frac{\sigma}{r}\right)^{12} - \left(\frac{\sigma}{r}\right)^{6}\right], & r \leq r_c, \\ 0, & r > r_c, \end{cases} \qquad [10]$$

where r is the interparticle distance, ϵ is the dispersion energy and the cutoff radius is set to $r_c = 2.5\sigma$. Analogous to Sec. A.2 of the main text, reference data is generated via GCMC simulations of 800 systems with randomized external conditions of which 500 are used for training and 150 respectively for validation and testing. We focus on the isothermal behavior of the supercritical fluid and hence set $k_BT = 1.5\epsilon$. The chemical potential varies uniformly in a range of $-8 \leq \beta\mu \leq 4$ and the external potential is generated as described in the main text, cf. Eq. (3).

To accomodate the longer-ranged interactions compared to the hard sphere fluid, the size of the density window to be input into the neural network is increased to $x_c = 4\sigma$ whilst keeping the design of the hidden layers unchanged (see Sec. A.3). The training results in a mean average error of 0.0035 and larger values of x_c led to no further improvement in the training statistics. The slight increase of the mean average error as compared to the hard sphere case (see Sec. A.4) can be attributed to noisier simulation data, which results from the decreased efficiency of GCMC method when simulating soft interactions with larger cutoff radius instead of hard spherical particles with an interaction range of σ.

After successfully training the neural functional for the Lennard-Jones fluid, we employ $c_1^\star(x;[\rho])$ in neural DFT to determine self-consistent density profiles for all 150 test systems. The Picard iteration proceeds without problems and analogously to Sec. C.1. The results are compared with the standard mean field DFT treatment of the Lennard-Jones fluid. Here, the repulsive part of Eq. (10) is approximated by a hard core interaction, for which we utilize the White Bear MkII FMT functional. An additive mean field contribution $F_{\mathrm{MF}}[\rho] = \int \mathrm{d}\mathbf{r} \int \mathrm{d}\mathbf{r}'\, \rho(\mathbf{r})\rho(\mathbf{r}')\phi_{\mathrm{att}}(|\mathbf{r}-\mathbf{r}'|)/2$ to the excess free energy functional incorporates

the attractive part $\phi_{\mathrm{att}}(r)$ of the Lennard-Jones potential. The function $\phi_{\mathrm{att}}(r)$ is equal to Eq. (10) for $r \geq r_{\mathrm{min}} = 2^{1/6}\sigma$ and it is set to $-\epsilon$ for $r < r_{\mathrm{min}}$.

Local and global deviations of both neural DFT and the analytic mean field DFT to the simulation reference data are presented in Fig. S4. The neglection of correlations in the mean field treatment leads to considerable errors across the whole test set. Contrarily, the neural DFT achieves close-to-simulation results and outperforms the analytic DFT by up to two orders of magnitude in the considered error measures.

This successful test demonstrates the transferability of our machine learning framework across particle models and indicates its utility especially for Hamiltonians which lack satisfactory analytic DFT treatments. Although the considered interparticle potential Eq. (10) is still short-ranged, we see much potential to extend our method to long-ranged interactions as occur e.g. in charged systems. The resulting algebraic decay of direct correlations could be tackled in various ways: i) It might be sufficient in some cases (e.g. for screened interactions) to simply extend the cutoff range x_c of the density input. ii) In order to achieve a better scaling of the number of input nodes with growing x_c, one could change the corresponding discretization of $\rho(x)$ to employ variably spaced sampling points instead of a fixed discretization interval. This would still enable to finely resolve the vicinity of the considered location x while also incorporating information about long-range density correlations. iii) An alternative approach emerges by treating the long-range behavior of $c_1(\mathbf{r};[\rho])$ analytically, similar to the treatment of the Hartree term in quantum DFT, see e.g. Ref. (11). Hence, the neural functional could be trained as is on the remaining short-ranged part of $c_1(\mathbf{r};[\rho])$ to recover full quasi-exact information about intrinsic correlations.

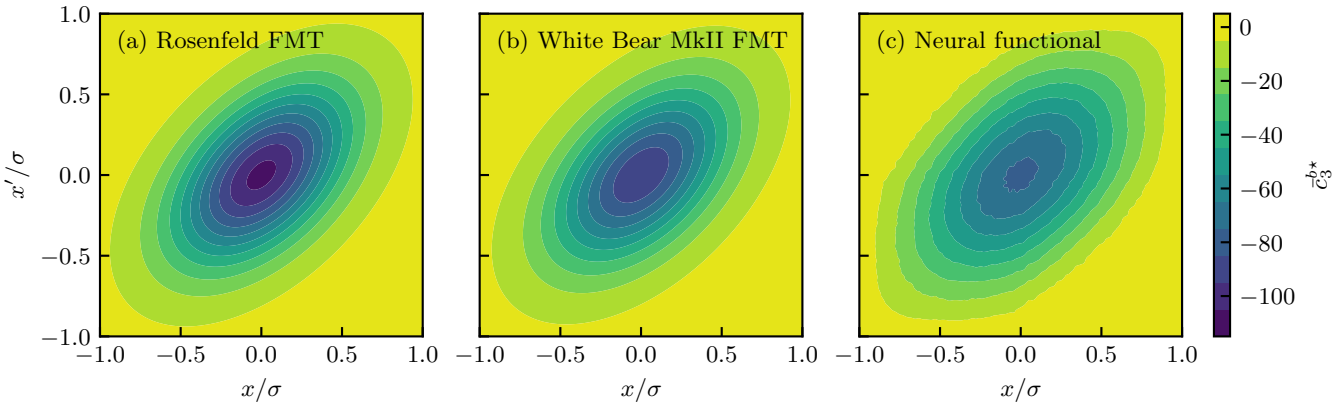

Fig. S1. The three-body direct correlation function is shown in bulk at density $\rho_b = 0.7\sigma^{-3}$. We depict (a) the Rosenfeld and (b) the White Bear MkII FMT results for the planar representation $\bar{c}_3^b(x, x')$, which were obtained analytically according to Eq. (2) by a cumulant expansion in Fourier space and a subsequent backtransform. Within our neural functional framework (c), $\bar{c}_3^{b\star}(x, x')$ is acquired via nested automatic differentiation of $c_1^\star(x; [\rho])$.

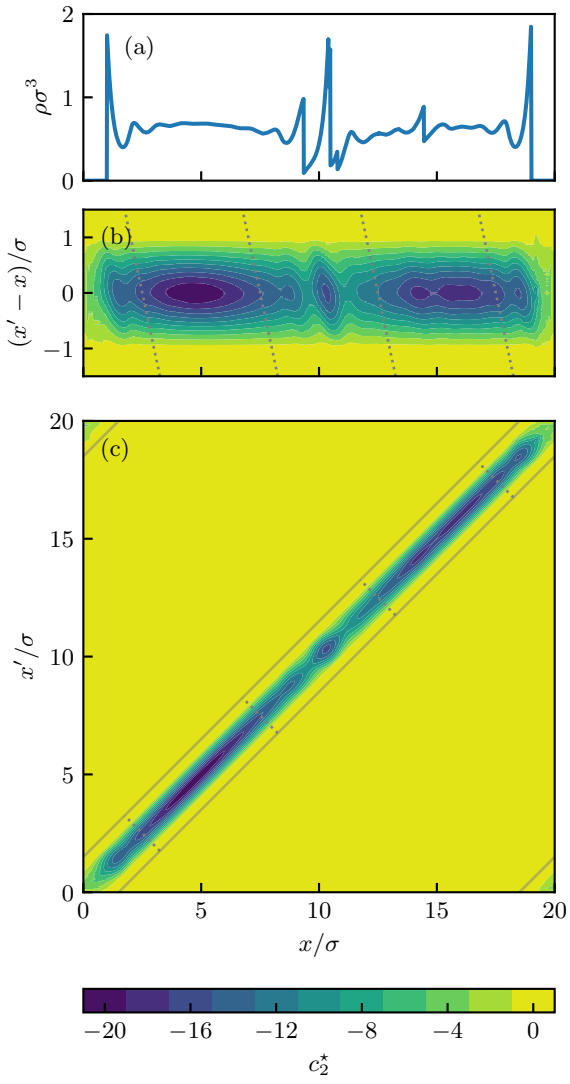

Fig. S2. We show (a) the density profile $\rho(x)$ of an inhomogeneous system of the test set and (b) the corresponding neural two-body direct correlation function, which is obtained for each position x with respect to $x'-x$. A linear transformation is applied to display $c_2^\star(x,x';[\rho])$ as a function of x and x' in panel (c). This transformation is visualized by corresponding gray lines in panels (b) and (c) which indicate the extent of the detailed view (solid) and slices where $x+x'=\mathrm{const.}$ (dotted). The results exemplify that the neural network reproduces the symmetry property Eq. (8) of the two-body direct correlation function very accurately.

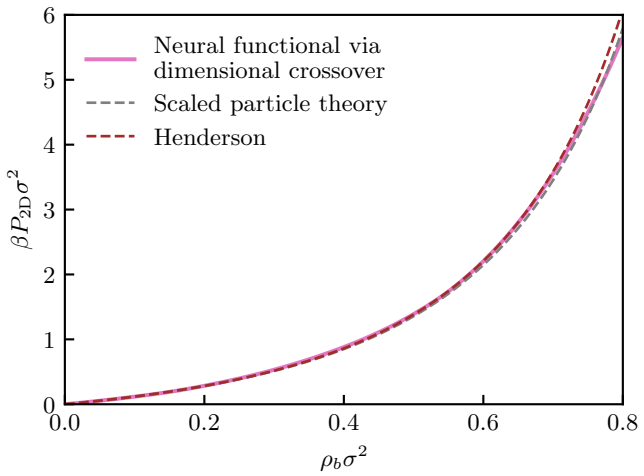

Fig. S3. The equation of state $P_{2D}(\rho_b)$ for two-dimensional hard disks is depicted, which is obtained from the neural functional via dimensional crossover. For comparison, we show analytic results according to scaled particle theory (9) and by Henderson (10). Although the training data for the three-dimensional hard sphere fluid did not cover narrow confinement within hard walls, $c_1^\star(0;[\rho])$ reproduces very reasonable behavior when applied to such quasi-two-dimensional situations and yields acceptable results for densities up to $\rho_b \approx 0.7\sigma^{-2}$.

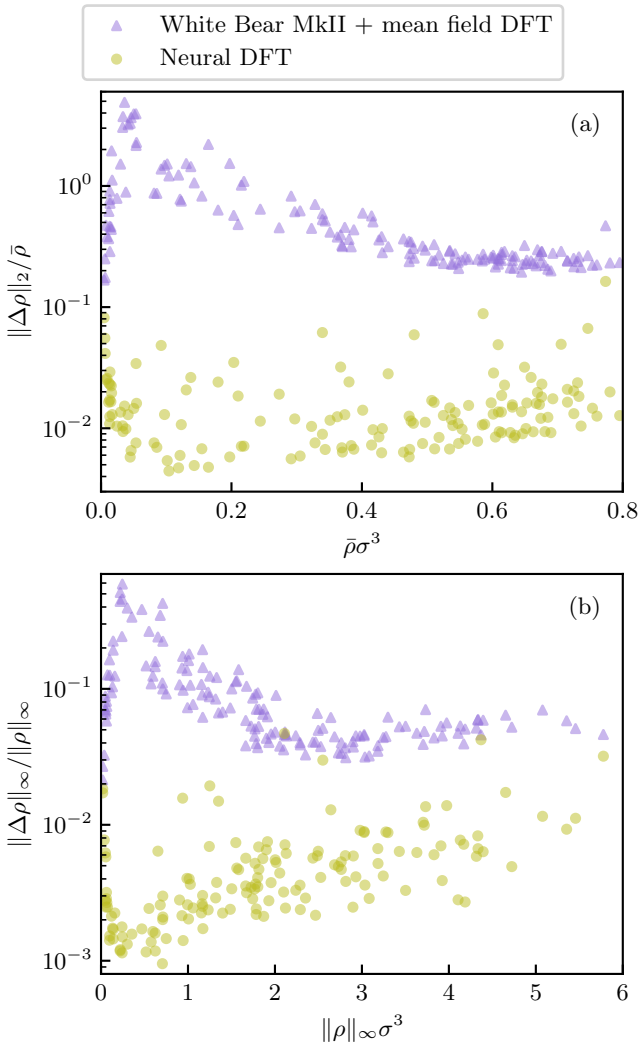

Fig. S4. Neural DFT (yellow circles) is compared to the standard mean field DFT (purple triangles) for the truncated Lennard-Jones fluid. As in Fig. 6, (a) the normalized L_2-norm $\|\Delta\rho\|_2/\bar{\rho}$ as a function of the mean density $\bar{\rho}$, and (b) the relative maximum norm $\|\Delta\rho\|_\infty/\|\rho\|_\infty$ as a function of the largest local density $\|\rho\|_\infty$ are considered. While considerable deviations to the reference profiles are observed for the hard sphere plus mean field treatment, neural DFT achieves almost simulation-like accuracy with global and local errors being decreased by up to two orders of magnitude.

References

1. JP Hansen, IR McDonald, *Theory of Simple Liquids With Applications to Soft Matter*. (Elsevier Science & Technology Books), (2013).
2. L Dixon, Automatic differentiation: Calculation of the Hessian in *Encyclopedia of Optimization*. (Springer US), pp. 133–137 (2008).
3. V Molinero, EB Moore, Water modeled as an intermediate element between carbon and silicon. *J. Phys. Chem. B* **113**, 4008–4016 (2008).
4. Y Rosenfeld, Free-energy model for the inhomogeneous hard-sphere fluid mixture and density-functional theory of freezing. *Phys. Rev. Lett.* **63**, 980–983 (1989).
5. E Kierlik, ML Rosinberg, Free-energy density functional for the inhomogeneous hard-sphere fluid: Application to interfacial adsorption. *Phys. Rev. A* **42**, 3382–3387 (1990).
6. S Phan, E Kierlik, ML Rosinberg, B Bildstein, G Kahl, Equivalence of two free-energy models for the inhomogeneous hard-sphere fluid. *Phys. Rev. E* **48**, 618–620 (1993).
7. H Hansen-Goos, R Roth, Density functional theory for hard-sphere mixtures: the White Bear version mark II. *J. Phys.: Condens. Matter* **18**, 8413–8425 (2006).
8. P Tarazona, Density functional for hard sphere crystals: A fundamental measure approach. *Phys. Rev. Lett.* **84**, 694–697 (2000).
9. H Reiss, HL Frisch, JL Lebowitz, Statistical mechanics of rigid spheres. *J. Chem. Phys.* **31**, 369–380 (1959).
10. D Henderson, A simple equation of state for hard discs. *Mol. Phys.* **30**, 971–972 (1975).
11. Y Zhou, J Wu, S Chen, G Chen, Toward the exact exchange-correlation potential: A three-dimensional convolutional neural network construct. *J. Phys. Chem. Lett.* **10**, 7264–7269 (2019).